Atmospheric Environment 45 (2011) 3454–3465

Contents lists available at ScienceDirect

Atmospheric Environment

journal homepage: www.elsevier.com/locate/atmosenv

# Application of MM5 in China: Model evaluation, seasonal variations, and sensitivity to horizontal grid resolutions

Yang Zhang [a,*], Shu-Hui Cheng [a,b], Yao-Sheng Chen [a], Wen-Xing Wang [b]

[a] Department of Marine, Earth, and Atmospheric Sciences, North Carolina State University, Raleigh, NC 27695, USA
[b] Environment Research Institute, Shandong University, Jinan, Shandong Province, PR China

ARTICLE INFO

*Article history:*
Received 17 November 2010
Received in revised form
7 February 2011
Accepted 2 March 2011

*Keywords:*
MM5
Meteorological model evaluation
Sensitivity to horizontal grid resolution
China

ABSTRACT

The rapid growth of energy consumption in conjunction with economic development during past decades in East Asia, especially China, caused severe air pollution problems at local and regional scales. Understanding of the meteorological conditions for air pollution is essential to the understanding of the formation mechanism of air pollutants and the development of effective emission control strategies to reduce air pollution. In this paper, the Fifth Generation National Center for Atmospheric Research (NCAR)/Pennsylvania State University (PSU) Mesoscale Model (MM5) modeling system is applied to simulate meteorological fields during selected six 1-month periods in 2007/2008 over a triple-nested modeling domain covering East Asia, the eastern China, and Shandong Province at horizontal grid resolutions of 36-, 12-, and 4-km, respectively. MM5 generally reproduces well the observations in the eastern China but performs worse in the western China and northeastern China. Largest biases occur in 2-m temperatures (T2) and wind speed and wind direction at 10-m in haze months (i.e., winter) and daily mean precipitation (Precip) in non-haze months (i.e., summer), due to limitations of the model in simulating snow cover and convective precipitation. Meteorological predictions agree more closely with observations at urban sites than those at the coastal and mountain sites where the model performance deteriorates because of complex terrains, influences of urban heat island effect and land/sea breezes, and higher elevations. Model results at 12-km in Shandong Province show an overall better performance than those at 4- or 36-km while the results at 4-km show worst performance due to inaccurate land use and the model's incapability in simulating meteorological processes at a fine scale.



## 1. Introduction

The population of 1330 millions in China accounts for 20% of the world's total population as of 2008. The rapid growth of energy consumption in conjunction with the economic development during the past 20 years in East Asia, especially China, has resulted in a dramatic increase of emissions of major trace gases and aerosols and subsequently severe air pollution at local and regional scales. Shandong Province, located in the northeast coast of China and adjacent to Korea and Japan across Bohai Sea, has the highest emissions of sulfur dioxide ($SO_2$), nitrogen oxides ($NO_x$), and particulate matter (PM) in China (http://zls.mep.gov.cn/hjtj/nb/2008tjnb/201004/t20100421_188500.htm). High emissions of air pollutants, especially those from coal combustions in winter, coupled with the complex terrain and anti-cyclone system in Shandong Province, have large impacts on urban and regional air quality. The most visible impact of air pollution is the haze, a brownish layer of pollutants from biomass burning and industrial emissions pervading in many regions such as most of the tropical Indian Ocean, South, Southeast and East Asia, which was found during the Indian Ocean Experiment (INDOEX) (UNEP and C[4], 2002) and known as "Asian Brownish Clouds" (Wu, 2005, 2006). Regional haze can directly impact temperature, precipitation, PM formation, visibility, human health, agriculture and sustainable development (Pope et al., 2004). Furthermore, the reduction of radiation and sunshine by haze that persists for a long time indirectly affects climate (Kaiser and Qian, 2002) and the meteorological transport of air pollutants that causes the vast extent haze to happen. The heavy haze occurs in the Pearl River Delta region of China where a number of observational and modeling studies have been conducted (e.g., Wang et al., 2003, 2006; Cao et al., 2004; Hagler et al., 2006; Andreae et al., 2008; Wu et al., 2008a; Garland et al., 2008; Xiao et al., 2009; Tan et al., 2009; Jung et al., 2009; Yu et al., 2010; Yue et al., 2010; Rose et al., 2010). These studies focused on characteristics of regional haze, the impact of regional haze on climate, the relationship between

* Corresponding author.
*E-mail address:* yang_zhang@ncsu.edu (Y. Zhang).

1352-2310/$ – see front matter © 2011 Elsevier Ltd. All rights reserved.
doi:10.1016/j.atmosenv.2011.03.019

emission types and regional haze, and transport of air pollutants. Studies on the impact of the regional haze in China or East Asia on precipitations, climate, and visibility reductions in other regions have also been conducted (e.g., Ramanathan et al., 2001; Yu et al., 2001; Kaiser and Qian, 2002; Wang et al., 2002; Radojevic, 2003; Ge, 2008; Liu et al., 2010a,b). For example, Ramanathan et al. (2001) studied the impact of haze on the climate in Indian or Southeast Asia and found that the absorbing haze decreased surface solar radiation, and also affected the rainfall pattern and hydrological cycle. The presence of haze and its optical properties in Indian have been studied (e.g., Franke et al., 2003; Mitra and Sharma, 2002). The impact of transport of regional haze in East Asia to Singapore and U.S. on local air quality has also been evaluated (e.g., Koe et al., 2001; Wang et al., 2009).

In this study, the Pennsylvania State University (PSU)/National Center for Atmospheric Research (NCAR) Mesoscale Modeling System Generation 5 version 3.7 (MM5) is applied to simulate meteorological conditions during haze and non-haze periods in China, their seasonal variations, and meteorological conditions during the 2008 Olympic Games. The Planetary Boundary Layer Model (PBL) and Land Surface Model (LSM) parameterizations are important to MM5 applications for air quality studies (Betts et al., 1997; Ku et al., 2001; Xiu and Pleim, 2001; Zhang et al., 2001; Athanassiadis et al., 2002; Pino et al., 2004; Miao et al., 2007, 2008; Misenis and Zhang, 2010). The Pleim-Xiu Land Surface Model (PX-LSM) of Pleim and Xiu (1995) with soil moisture nudging can provide more accurate near surface meteorology in air quality modeling and precipitation simulations than the Noah Land surface scheme (Pleim et al., 2001; Xiu and Pleim, 2001). In this paper, nested simulations using MM5 with the PX-LSM with soil moisture and temperature nudging, reanalysis nudging, and observational nudging are conducted and evaluated using reanalysis data and in-situ observational data. Our objectives are to evaluate MM5 performance in reproducing observed meteorological variables during regional haze and non-haze period and examine their seasonal variations and implications on air quality. Air quality simulations using the U.S. EPA Community Multiscale Air Quality (CMAQ) modeling system with MM5 predictions in this study are described in Liu et al. (2010a,b), and Xing et al. (2011).

## 2. Model configurations and datasets for model evaluation

### 2.1. Episode and model configurations

Six 1-month periods in 2007 and 2008 are selected for MM5 simulations: December, 2007 and January, April, July, August, and October 2008. The frequency of regional haze in winter is much higher than that in other seasons, so the simulations of December 2007 and January 2008 are used to represent the time period with regional haze; the simulations of January, April, July and October are used to understand the seasonal variation of meteorological process in China, especially in the eastern China where the air pollution is the most severe; the simulation of August is used to understand the meteorological conditions and provide meteorological inputs for CMAQ to evaluate the impact of the control of emissions on air quality during the period of the 2008 Olympics games in China, as compared with that before the 2008 Olympics games in July.

The modeling domains consist of a $36 \times 36$ km$^2$ domain covering East Asia, including Korea, Japan, and China, a $12 \times 12$ km$^2$ nested domain covering the eastern China, including Beijing, Tianjin, Hebei, Henan, Anhui, Shanghai, South of China and Shandong Province, and a $4 \times 4$ km$^2$ nested domain covering Shandong Province. Fig. 1 shows the triple-nested domains. For all domains, 23 layers are used for MM5 simulations extending from surface to tropopause (14.6 km) with about 36 m in the first layer. Two sets of publicly available reanalysis data (i.e., The National Centers for Environmental Prediction (NCEP)—Final analysis data (FNL) and Global Forecast System (GFS)) are used to obtain the best dataset for initial and boundary conditions (IC and BC). The NCEP data have a horizontal resolution of $1^\circ \times 1^\circ$ for every 6-h interval, whereas the GFS data have a horizontal resolution of $0.5^\circ \times 0.5^\circ$ for every 3-h interval. The terrain height and vegetation/land use data are taken from the 25-category USGS Vegetation Data derived from raw data with 30 s resolution (corresponding to 0.925 km) ftp://ftp.ucar.edu/mesouser/MM5V3/TERRAIN_DATA/. For other types of data such as land–water mask, soil, vegetation fraction, and annual deep soil temperature, the data with resolutions of 10, 5, and 2 min (corresponding to 18.5 km, 9.25 km, and 3.7 km, respectively) are used when available for the 36-km, 12-km, and 4-km simulation domains, respectively, otherwise

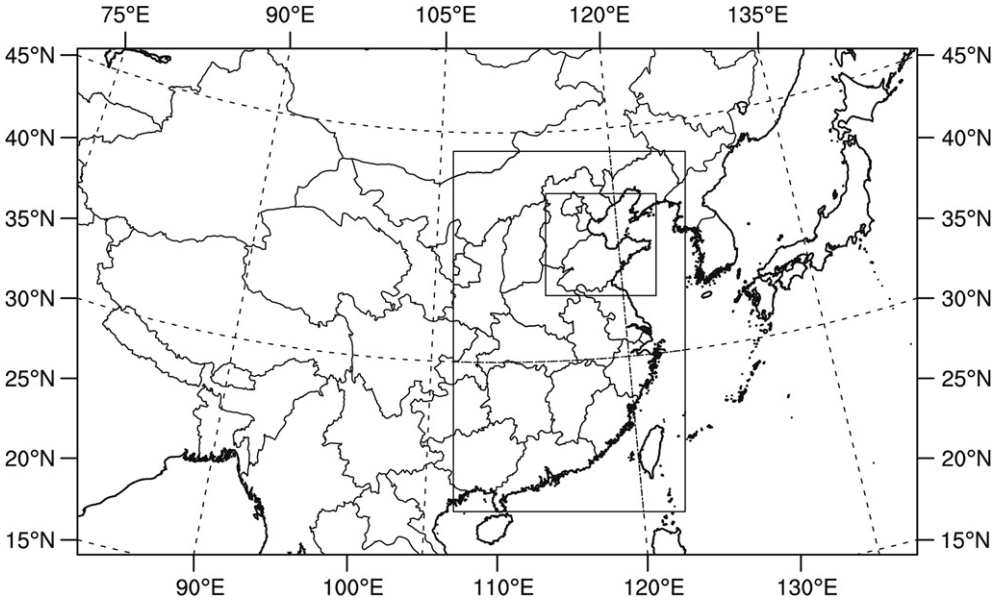


**Fig. 1.** The triple-nested modeling domains at 4-km (Shandong), 12-km (East China), and 36-km (China).

data at a coarser resolution will be used. For example, vegetation fraction data is only available at a 10 min resolution and annual deep soil temperature data is only available at a resolution of 1°. Table 1 shows the physics configurations used in model simulations. Four Dimensional Data Assimilation (FDDA) used in these simulations includes deep soil nudging, and reanalysis and observational nudging. The NCEP Automated Data Processing (ADP) Global Upper Air Observation Subsets with dataset numbers DS351.0 and DS461.0 obtained from NCAR/Scientific Computing Division (SCD)/Data Support Section (DSS) are used for the analysis and observational nudging. MM5 model simulations are conducted at 36- and 12-km over China and the eastern China for six one-month periods (i.e., December 2007, January, April, July, August and October 2008) and at 4-km over Shandong Province for two one-month periods (i.e., December 2007 and January 2008). The MM5 simulations started on November 23 to allow 7 days as spin up days to reduce the effect of IC on meteorology and CMAQ.

### 2.2. Datasets and evaluation protocols

Global Surface Data from the National Climatic Data Center (NCDC) available every 6-h at 358 sites in China are used to evaluate model results. Additional measurements data from Shangdong University for sites in Shangdong province during Dec. 2007 and Jan. 2008 are also used. The meteorological parameters evaluated focus on five major variables that affect air pollution: 2-m temperature (T2), 2-m relative humidity (RH2), 10-m wind speed (WSP10), 10-m wind direction (WDR10), and daily mean precipitation (Precip). Simulation results are compared with observations in terms of spatial distribution, temporal variations, and performance statistic following the evaluation protocol of Zhang et al. (2006) and Wu et al. (2008b). The statistics evaluated include correlation coefficient ($R$), Mean Bias (MB), Root Mean Square Error (RMSE), Normalized mean bias (NMB), and Normalized mean error (NME).

## 3. Simulation results

### 3.1. Evaluation of impact of different datasets for IC and BC

Two high − resolution datasets (NCEP FNL ($1 \times 1°$) and GFS ($0.5° \times 0.5°$)) are used to generate IC and BC for MM5 at 36-km to evaluate the impact of different initialization datasets on MM5 simulation. Since the largest cold bias in temperatures is found for Dec. 2007 and Jan. 2008, the two months are selected for this evaluation. Table 2 compares the performance statistics for T2, RH2, WSP10, WDR10, and Precip for the 36-km simulations using these two datasets for the two months. The simulations with the GFS dataset have larger MB, RMSE, NMB and NME than those with the FNL dataset. For example, the MBs of T2 are −1.7 and −2.2 °C with the FNL dataset and −3.0 and −3.7 °C with the GFS dataset in Dec. 2007 and Jan. 2008, respectively. The systematical underpredictions in T2 are likely due to the model limitations in simulating snow cover and the fact that the spin up period may still be too short, particularly in winter months. For RH2, the simulation with the FNL dataset gives larger absolute values of MB and NMB in Dec. but larger absolute values of MB and NMB in Jan. The simulation with the FNL dataset gives better performance for WSP10, WDR10, and Precip in both months than that with the GFS dataset. As shown in Fig. 2, differences exist in simulated spatial distributions with both datasets. For example, compared with results with the FNL dataset, the simulation with the GFS dataset gives a larger cold bias in T2, particularly in the eastern China, lower RH2 values in the southern China, slightly lower Precip amounts over land but higher over the Pacific ocean. Overall, the simulations with the FNL dataset perform better in terms of domain-wide statistics and spatial distribution; it is therefore used for IC and BC for all the simulations.

**Table 1**
MM5 model configurations used in this study.

| Process | Parameterization or Scheme |
|---|---|
| Land Surface Model | Pleim-Xiu LSM |
| Planetary Boundary Layer Model | Pleim-Xiu |
| Cloud Microphysics | Mixed-Phase |
| Cumulus Scheme | Kain-Fritcsh (KF) |
| Shallow Convection | No Shallow Convection |
| Longwave Radiation | Dudhia |
| Shortwave Radiation | Dudhia |
| Analysis Nudging | Yes |
| Nudging coefficients for Temperature | $3.0 \times 10^{-4}$ s$^{-1}$ |
| Nudging coefficients for Moisture | $1.0 \times 10^{-4}$ s$^{-1}$ |
| Nudging coefficients for Wind (u and v) | $3.0 \times 10^{-4}$ s$^{-1}$ |
| Observational Nudging | Yes |
| Soil Nudging | Yes |

### 3.2. Evaluation of six-month simulations at 36- and 12-km

#### 3.2.1. Spatial distributions and domain-wide statistics

Fig. 3 shows similar overlay plots for T2, RH2, WSP10, and precipitation from the 36-km simulation with the FNL dataset but for the remaining four months (Apr., Jul., Aug., and Oct.). The spatial distributions at 12-km are not shown because they are similar to those at 36-km. The domain-wide performance statistics for all six months are summarized in Table 2. The seasonal variation of observed T2 is overall captured; despite some differences in the magnitudes in some regions. Underpredictions in T2 occur at the NCDC sites in the western China and overpredictions occur in the eastern China in all months. Underpredictions dominate over overpredictions, resulting in NMBs of −28 to −3% and MBs ranging from −2.2 °C to −0.6 °C. Simulated T2 agree well with observations with MBs within 1 °C except for December 2007 and January 2008. The largest cold bias occurs in both months in the western China where the Mt. Himalayas with thick snows is located, which is consistent with Ma et al. (2008). Such a large cold bias indicates the incapability of MM5 in reproducing observed snow cover. Simulated T2 values and their spatial variations at 36-km in Jul. and Aug. are closer to observations with NMBs of −4 to −3% and MBs of −0.8 °C to −0.6 °C. Observed RH2 values in summer are higher than those in other months, which is reproduced by MM5. Simulated RH2 values agree well with observations in most of China but underpredictions dominate the domain-wide statistics in all months except for Jan. with NMBs of −9.0% to 3.0% and MBs of −5.9 to 1.8%. RH2 is overpredicted in Dec. and Jan. and underpredicted in other months in the northeast of China. Variation of observed WSP10 from season to season and from region to region is not evident. WSP10 in the western China is overpredicted with NMBs and MBs ranging from 40 to 86% and 1.0 to 2.2 m s$^{-1}$, respectively in all months, which may blow too much amount of pollutants out of the domain, partially responsible for the underpredictions of concentrations of air pollutants such as $SO_2$ and $NO_2$ (Liu et al., 2010a). Simulated WSP10 is the highest in spring, consistent with observations. This can partially explain simulated higher $SO_2$ concentrations in Oct. than in Apr. due to lower ventilation rates in Oct., as shown in Liu et al. (2010a). Simulated WDR10 deviates from observations by −31.5 to −18.8°. One limitation of evaluating WDR10 is that it is a vector, the numeric values of differences between the observations and predictions may not reflect well the actual differences in the wind rose plots when those values are greater than 180°, as indicated in Zhang et al. (2006). Observed precipitation in the eastern China is larger than that in other regions. Heavy rain resulted from convective clouds/precipitations

**Table 2**
Perform statistics of MM5 predictions at 36-km over China.

| | | Month | MeanObs | MeanMod | $R^a$ | MB[a] | RMSE[a] | NMB(%)[a] | NME(%)[a] |
|---|---|---|---|---|---|---|---|---|---|
| T2 | GFS | Dec | 8.9 | 5.9 | 0.7 | −3.0 | 5.3 | −34.1 | 44.8 |
| | | Jan | 7.6 | 3.9 | 0.6 | −3.7 | 6.7 | −48.8 | 63.1 |
| | FNL | Dec | 8.7 | 7.0 | 0.8 | −1.7 | 4.3 | −19.0 | 35.0 |
| | | Jan | 7.9 | 5.7 | 0.7 | −2.2 | 5.4 | −28.0 | 47.0 |
| | | Apr | 13.9 | 12.8 | 0.8 | −1.0 | 4.3 | −8.0 | 22.0 |
| | | Jul | 19.6 | 19.0 | 0.8 | −0.6 | 4.1 | −3.0 | 16.0 |
| | | Aug | 18.9 | 18.1 | 0.8 | −0.8 | 3.9 | −4.0 | 16.0 |
| | | Oct | 14.1 | 12.9 | 0.9 | −1.2 | 3.8 | −9.0 | 20.0 |
| RH2 | GFS | Dec | 60.1 | 58.4 | 0.6 | −1.7 | 23.8 | −2.8 | 30.1 |
| | | Jan | 61.9 | 66.4 | 0.5 | 4.5 | 24.7 | 7.2 | 30.0 |
| | FNL | Dec | 60.2 | 57.9 | 0.7 | −2.3 | 21.1 | −4.0 | 27.0 |
| | | Jan | 60.1 | 61.9 | 0.6 | 1.8 | 22.9 | 3.0 | 29.0 |
| | | Apr | 53.5 | 53.0 | 0.7 | −0.5 | 21.0 | −1.0 | 29.0 |
| | | Jul | 67.7 | 64.0 | 0.7 | −3.7 | 19.6 | −6.0 | 22.0 |
| | | Aug | 68.8 | 64.9 | 0.7 | −3.9 | 19.1 | −6.0 | 21.0 |
| | | Oct | 64.3 | 58.4 | 0.7 | −5.9 | 21.4 | −9.0 | 25.0 |
| WSP10 | GFS | Dec | 2.4 | 4.9 | 0.4 | 2.5 | 3.7 | 101.5 | 118.9 |
| | | Jan | 2.6 | 4.8 | 0.4 | 2.2 | 3.3 | 85.7 | 102.3 |
| | FNL | Dec | 2.4 | 4.0 | 0.4 | 1.5 | 2.7 | 63.0 | 86.0 |
| | | Jan | 2.6 | 4.8 | 0.4 | 2.2 | 3.3 | 86.0 | 102.0 |
| | | Apr | 3.0 | 4.6 | 0.5 | 1.5 | 2.9 | 50.0 | 73.0 |
| | | Jul | 2.6 | 3.6 | 0.4 | 1.0 | 2.4 | 40.0 | 71.0 |
| | | Aug | 2.4 | 3.5 | 0.4 | 1.1 | 2.3 | 45.0 | 74.0 |
| | | Oct | 2.5 | 3.8 | 0.4 | 1.4 | 2.5 | 56.0 | 80.0 |
| WDR10 | GFS | Dec | 215.7 | 151.6 | 0.0 | −64.2 | 192.5 | −29.7 | 62.7 |
| | | Jan | 211.3 | 180.7 | 0.2 | −30.7 | 183.6 | −14.5 | 52.9 |
| | FNL | Dec | 215.4 | 189.6 | 0.2 | −25.8 | 182.8 | −12.0 | 50.0 |
| | | Jan | 211.4 | 180.7 | 0.2 | −30.7 | 183.6 | −15.0 | 53.0 |
| | | Apr | 204.2 | 185.4 | 0.2 | −18.8 | 162.7 | −9.0 | 46.0 |
| | | Jul | 195.2 | 172.7 | 0.2 | −22.5 | 162.0 | −12.0 | 48.0 |
| | | Aug | 196.0 | 170.5 | 0.2 | −25.6 | 170.1 | −13.0 | 50.0 |
| | | Oct | 207.6 | 176.1 | 0.2 | −31.5 | 181.0 | −15.0 | 50.0 |
| Precip | GFS | Dec | 3.0 | 2.1 | 0.2 | −0.9 | 7.6 | −31.5 | 120.3 |
| | | Jan | 3.7 | 4.0 | 0.0 | 0.4 | 40.0 | 10.0 | 156.2 |
| | FNL | Dec | 3.0 | 2.4 | 0.3 | −0.6 | 6.4 | −20.0 | 115.0 |
| | | Jan | 3.5 | 3.9 | 0.4 | 0.4 | 7.0 | 11.0 | 110.0 |
| | | Apr | 7.2 | 4.7 | 0.3 | −2.5 | 15.2 | −34.0 | 110.0 |
| | | Jul | 11.8 | 8.9 | 0.2 | −2.8 | 26.3 | −24.0 | 118.0 |
| | | Aug | 10.9 | 7.6 | 0.2 | −3.2 | 23.2 | −30.0 | 120.0 |
| | | Oct | 6.5 | 5.6 | 0.3 | −1.0 | 14.4 | −15.0 | 118.0 |

Precip − Precipitation, RH2 − 2 m Relative Humidity, T2 − 2 m Temperature, WDR10 − 10 m Wind Direction, WSP10 − 10 m Wind Speed.
[a] $R$ − Correlation Coefficient, MB − Mean Bias, RMSE − Root Mean Square Error, NMB − Normalized mean bias, NME − Normalized mean error.

occurs in summer in this region, which leads to the lowest $PM_{10}$ concentrations in Jul. among all months, as reported in Liu et al. (2010a). The daily mean precipitation (convective and non-convective) is underpredicted in most of China with NMBs of −34% to 11% and MBs of −3.2 mm to 0.4 mm in all months except for January during which four episodes with severe and persistent snow storms occurring from 10 January to 2 February (Gao, 2009). The circulation patterns in Dec. and Jan. are similar but the snow storms in Jan. are heavier than those in Dec. which may explain the opposite trend in the simulated precipitation in both months. Compared with other meteorological variables, the observational data for precipitation are sparse in some regions such as the Tibetan Plateau, which introduces some uncertainties in model performance in such regions.

The performance statistics are calculated using observations at all sites within the 12-km domain from the simulations at 36- and 12-km to evaluate the sensitivity of MM5 predictions to horizontal grid resolution over the eastern China, as shown in Table 3. Compared with results at 36-km, the nested 12-km simulations for T2 are slightly better than those at 36-km in all the months except slightly worse in January and July with MBs ranging from −1.2 °C to 0.6 °C at 36-km and −1.4 °C to 0.7 °C at 12-km. The NMBs and MBs in RH2 are smaller at 12-km in winter and spring but slightly larger in summer and fall. The NMBs and MBs for WSP10 and WDR10 at 12-km are generally smaller than those at 36-km, likely because the model performance over the eastern domain at 36-km is somewhat affected by its incapability in accurately simulating wind patterns around Mt. Himalayas located at the western China. The MBs in precipitation range from −5.1 mm to −0.5 mm at 36-km and from −4.0 mm to −0.6 mm at 12-km, also with better agreement with observations at 12-km.

### 3.2.2. Temporal variations

To understand model performance at local scale, four major cities (i.e., Beijing, Xi'an, Shanghai, and Guangzhou) are selected to represent different regions of China for detailed temporal variation analyses for the six months at 36- and 12-km. Beijing is the largest city in China featured with hot humid summers and cold dry winters with virtually no precipitation. The winter cold weather is due to Siberian air masses that move southward across the Mongolian Plateau. The summers are hot owing to warm and humid monsoon winds from the southeast, bringing most of its annual precipitation. It suffers severe air pollution problems as a consequence of large population and fast economic growth. The emissions of major air pollutants were controlled to ensure a good air quality during the Olympics Games in August 2008. Xi'an is the biggest city in the western China. It is situated in the Guanzhong Plain, borders on the Loess Plateau to the north and the Qinling Mountains to the south. The weather is affected by continental monsoon. The air is very cold and dry and the concentrations of PM

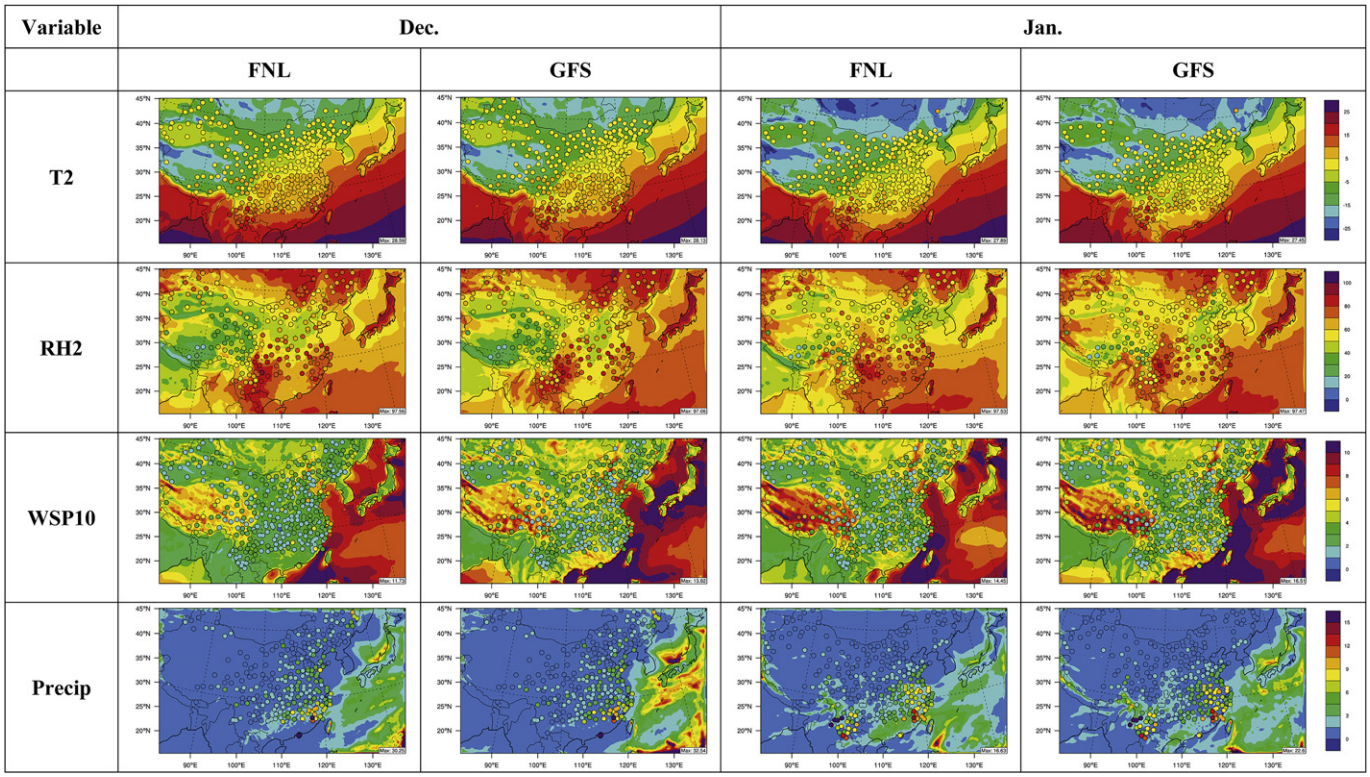


**Fig. 2.** Simulated monthly-average meteorological parameters overlaid with NCDC observations (symbol as circle) during 12/01/2007 to 01/31/2008 initiated with FNL and GFS datasets.

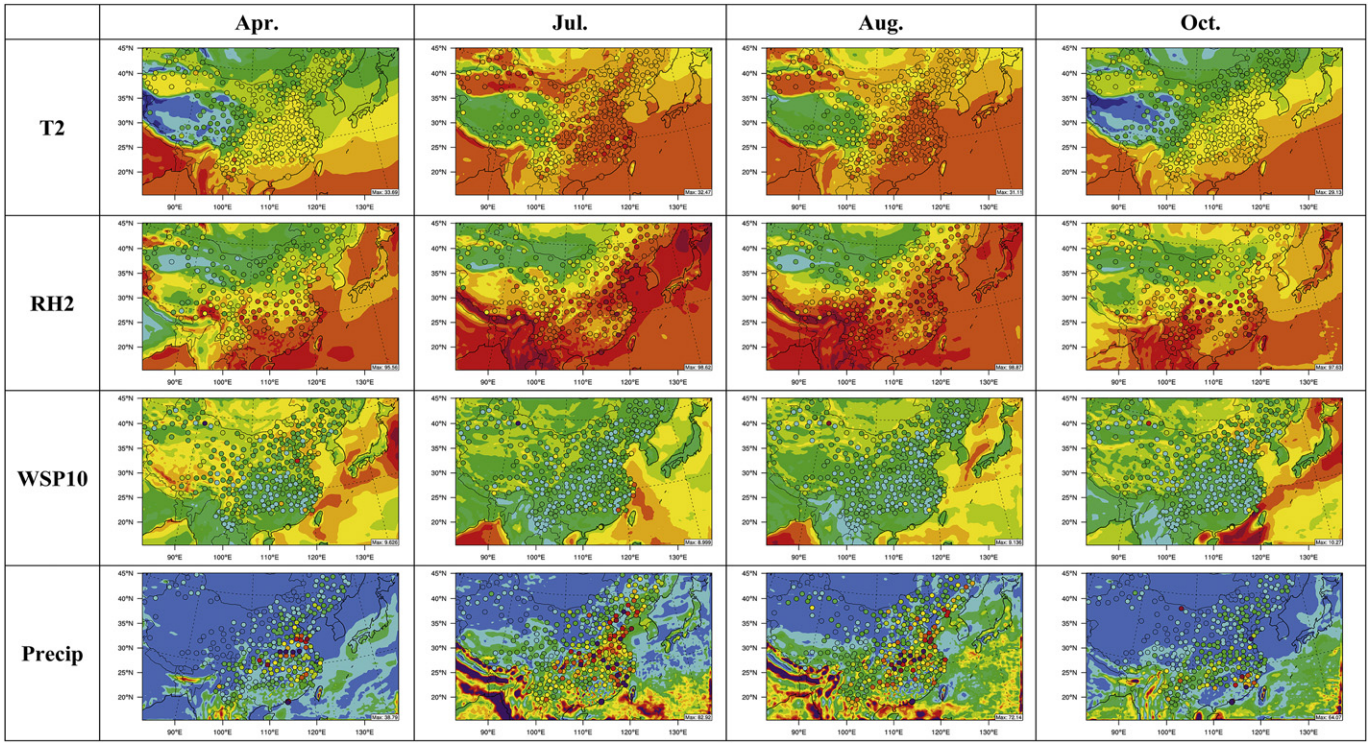


**Fig. 3.** Spatial distributions of simulated T2, RH2, WSP10, and Precipitation at 36-km overlaid with observations (symbols as circle). The FNL datasets were used to initiate the simulations.

**Table 3**
Performance statistics of MM5 simulations at 36- and 12-km over the eastern China.

| | Month | MeanObs | | MeanMod | | $R^a$ | | MB[a] | | RMSE[a] | | NMB(%)[a] | | NME(%)[a] | |
|---|---|---|---|---|---|---|---|---|---|---|---|---|---|---|---|
| | | 36 km | 12 km | 36 km | 12 km | 36 km | 12 km | 36 km | 12 km | 36 km | 12 km | 36 km | 12 km | 36 km | 12 km |
| T2 | Dec | 7.4 | 8.5 | 6.3 | 7.3 | 0.7 | 0.8 | −1.1 | −1.1 | 3.9 | 3.8 | −14.2 | −13.5 | 35.7 | 29.1 |
| | Jan | 7.5 | 7.5 | 6.3 | 6.1 | 0.7 | 0.7 | −1.2 | −1.4 | 4.9 | 4.8 | −16.0 | −19.0 | 41.0 | 38.0 |
| | Apr | 14.9 | 14.9 | 14.8 | 14.8 | 0.9 | 0.9 | −0.2 | −0.2 | 3.2 | 3.1 | −1.0 | −1.0 | 16.0 | 15.0 |
| | Jul | 22.1 | 22.1 | 22.6 | 22.7 | 0.6 | 0.6 | 0.6 | 0.7 | 3.2 | 3.1 | 3.0 | 3.0 | 10.0 | 10.0 |
| | Aug | 21.2 | 21.2 | 21.4 | 21.4 | 0.7 | 0.7 | 0.2 | 0.2 | 3.0 | 2.9 | 0.9 | 1.1 | 10.2 | 9.8 |
| | Oct | 15.8 | 15.8 | 15.3 | 15.3 | 0.9 | 0.9 | −0.5 | −0.4 | 3.0 | 2.9 | −3.0 | −3.0 | 14.0 | 13.0 |
| RH2 | Dec | 72.4 | 69.9 | 60.2 | 62.3 | 0.6 | 0.6 | −12.2 | −7.6 | 19.9 | 20.1 | −16.8 | −10.2 | 24.8 | 21.4 |
| | Jan | 68.6 | 68.6 | 62.2 | 63.0 | 0.7 | 0.7 | −6.3 | −5.6 | 19.6 | 18.6 | −9.0 | −8.0 | 22.0 | 20.0 |
| | Apr | 67.4 | 67.4 | 61.1 | 61.2 | 0.8 | 0.8 | −6.3 | −6.2 | 18.1 | 18.2 | −9.0 | −9.0 | 20.0 | 20.0 |
| | Jul | 75.8 | 75.8 | 69.5 | 67.9 | 0.7 | 0.7 | −6.4 | −7.9 | 16.6 | 17.4 | −8.0 | −11.0 | 20.0 | 18.0 |
| | Aug | 76.6 | 76.6 | 69.5 | 67.3 | 0.7 | 0.6 | −7.1 | −9.3 | 16.9 | 18.8 | −9.3 | −12.1 | 16.9 | 18.9 |
| | Oct | 70.4 | 70.4 | 60.9 | 60.4 | 0.7 | 0.7 | −9.5 | −10.0 | 19.8 | 20.4 | −14.0 | −14.0 | 21.0 | 22.0 |
| WSP10 | Dec | 2.5 | 2.6 | 3.7 | 3.8 | 0.5 | 0.5 | 1.1 | 1.2 | 2.4 | 2.3 | 44.8 | 47.1 | 72.4 | 71.1 |
| | Jan | 2.7 | 2.7 | 4.6 | 4.1 | 0.5 | 0.5 | 1.9 | 1.4 | 2.9 | 2.4 | 71.0 | 50.0 | 87.0 | 71.0 |
| | Apr | 3.1 | 3.1 | 4.3 | 4.3 | 0.5 | 0.5 | 1.3 | 1.2 | 2.5 | 2.6 | 41.0 | 39.0 | 65.0 | 63.0 |
| | Jul | 2.7 | 2.7 | 3.6 | 3.6 | 0.4 | 0.5 | 0.9 | 0.9 | 2.2 | 2.2 | 34.0 | 32.0 | 64.0 | 63.0 |
| | Aug | 2.5 | 3.1 | 3.4 | 4.3 | 0.5 | 0.5 | 0.9 | 1.2 | 2.2 | 2.5 | 36.8 | 38.5 | 66.4 | 62.6 |
| | Oct | 2.5 | 2.5 | 3.7 | 3.6 | 0.5 | 0.5 | 1.2 | 1.1 | 2.3 | 2.2 | 49.0 | 45.0 | 73.0 | 69.0 |
| WDR10 | Dec | 215.4 | 211.8 | 173.0 | 177.8 | 0.2 | 0.2 | −42.4 | −34.0 | 190.6 | 190.5 | −19.7 | −16.0 | 53.8 | 51.3 |
| | Jan | 205.5 | 205.5 | 162.0 | 165.1 | 0.2 | 0.2 | −43.5 | −40.4 | 197.2 | 195.3 | −21.0 | −20.0 | 58.0 | 57.0 |
| | Apr | 198.1 | 198.1 | 172.5 | 171.8 | 0.2 | 0.2 | −25.5 | −26.3 | 167.0 | 167.8 | −13.0 | −13.0 | 45.0 | 44.0 |
| | Jul | 192.7 | 192.7 | 168.5 | 168.8 | 0.2 | 0.2 | −24.2 | −23.9 | 163.2 | 161.7 | −13.0 | −12.0 | 45.0 | 45.0 |
| | Aug | 193.5 | 193.5 | 166.8 | 167.3 | 0.2 | 0.2 | −26.7 | −26.2 | 176.2 | 176.9 | −13.8 | −13.5 | 48.9 | 49.1 |
| | Oct | 207.0 | 207.0 | 167.1 | 168.5 | 0.2 | 0.2 | −39.9 | −38.5 | 196.4 | 195.5 | −19.0 | −19.0 | 52.0 | 51.0 |
| Precip | Dec | 3.5 | 3.4 | 2.2 | 2.3 | 0.2 | 0.3 | −1.3 | −1.1 | 6.5 | 6.5 | −36.6 | −31.9 | 110.4 | 109.3 |
| | Jan | 4.0 | 4.0 | 3.5 | 3.4 | 0.4 | 0.3 | −0.5 | −0.6 | 6.6 | 6.8 | −13.0 | −16.0 | 98.0 | 98.0 |
| | Apr | 9.0 | 9.0 | 5.3 | 6.2 | 0.3 | 0.2 | −3.7 | −2.9 | 17.9 | 22.0 | −41.0 | −32.0 | 101.0 | 109.0 |
| | Jul | 14.8 | 14.8 | 11.2 | 13.2 | 0.2 | 0.1 | −3.7 | −1.6 | 33.1 | 43.3 | −25.0 | −11.0 | 123.0 | 139.0 |
| | Aug | 14.3 | 14.3 | 9.2 | 10.3 | 0.2 | 0.2 | −5.1 | −4.0 | 29.2 | 35.7 | −35.5 | −28.1 | 117.3 | 126.3 |
| | Oct | 7.4 | 7.4 | 5.4 | 5.5 | 0.3 | 0.2 | −2.0 | −1.9 | 15.3 | 18.2 | −27.0 | −26.0 | 112.0 | 117.0 |

Precip – Precipitation, RH2 – 2 m Relative Humidity, T2 – 2 m Temperature, WDR10 – 10 m Wind Direction, WSP10 – 10 m Wind Speed.
[a] $R$ – Correlation Coefficient, MB – Mean Bias, RMSE – Root Mean Square Error, NMB – Normalized mean bias, NME – Normalized mean error.

are higher in winter than those in other seasons (Zhang et al., 2002). Shanghai, located in the eastern China, has very cold and humid winters with few snowfall and hot and humid summers. June and July are the "plum rain season", characterized by gloomy and rainy weather. It is a center of economy in China where the rapid economic development has resulted in severe air pollution (Ye et al., 2003). Guangzhou is one of the major cities in the Pearl River Delta region in the southern China with sufficient sunshine and rainfall, and little frost and snow where the heavy haze often occurs (Wang et al., 2003; Cao et al., 2004; Hagler et al., 2006; Wu et al., 2008a).

Figs. 4–8 show temporal variations of T2, RH2, WSP10, WDR10, and Precip in the four cities during the six months. In Beijing, simulated temperatures during all months generally agree well with observations in terms of diurnal variations and magnitudes, although the minimal temperatures are underpredicted in Dec. and Jan. because MM5 could not capture well snow covers, and the simulated maximum temperatures are overpredicted in Jul., Aug., and Oct., likely due to overpredicted shortwave radiation. In Xi'an, the observed temperatures are similar in magnitude to those in Beijing but lower than those in Shanghai and Guangzhou during most of time. Maximum temperatures agree well with observations in Apr., Jul., and Aug. but are overpredicted in Dec., Jan., and Oct. during which overcast and cloudy weather often occurred but MM5 may have underpredicted cloud coverage. In Shanghai and Guangzhou, simulated temperatures capture well the observed temporal variations except for Jan. in Shanghai during which the minimum temperatures are underpredicted and for Apr. in Guangzhou with the maximum temperatures are overpredicted. Overall simulated temperatures at 36- and 12-km are fairly consistent in all months at all sites except for Shanghai in winter, which may be due to model's incapability in accurately simulate air-surface exchanges over unique complex topography and local weather patterns that are influenced by urban heat island effect and land/sea breezes. No direct measurements of RH2 were available, so RH2 is calculated based on measured dew point and pressure. In Beijing, the simulated minimum RHs capture well with observations but the maximum RHs are underpredicted in all the months. Observation-derived RH2 are not available due to the lack of dew point and/or pressure observations in Xi'an. MM5 at 12-km tends to give higher maximum and minimum RHs than at 36-km in winter and spring in both Beijing and Xi'an. In Shanghai, the simulations at 36-km and 12-km can capture the high and low RH2 values except in Jan. and Dec. with underpredictions in the minimum RHs. In Guangzhou, the observed maximum RHs are underpredicted in Dec. but captured well by the model in other months. The minimum RHs are underpredicted except in Oct. for which simulated RHs agree well with observations. The RH2 predictions at the two grid resolutions are generally consistent for most months at all sites. WSP10 are predominantly overpredicted at all sites during most of time, with better agreement in summer and fall than in winter and spring. Large deviations from observations exist in the simulated WDR10 in Guangzhou, with better performance at other sites. MM5 performs the worst in terms of WSP10 and WDR10 at some sites when calm wind conditions dominated (e.g., in Dec. and Jan. in Xi'an, Shanghai, and Guangzhou). The observed precipitation amounts in Beijing are smaller than those in Shanghai and Guangzhou, which is reproduced by MM5 (note that no observed precipitation amounts are available at Xi'an). The seasonality in precipitation is also reproduced in the three cities (e.g., heavier precipitation in summer and fall than winter in Beijing and Guangzhou). MM5 tends to overpredict precipitations in Shanghai and Guangzhou during summer, during which convection precipitation dominates. This is because too frequent afternoon convective rainfall and/or an

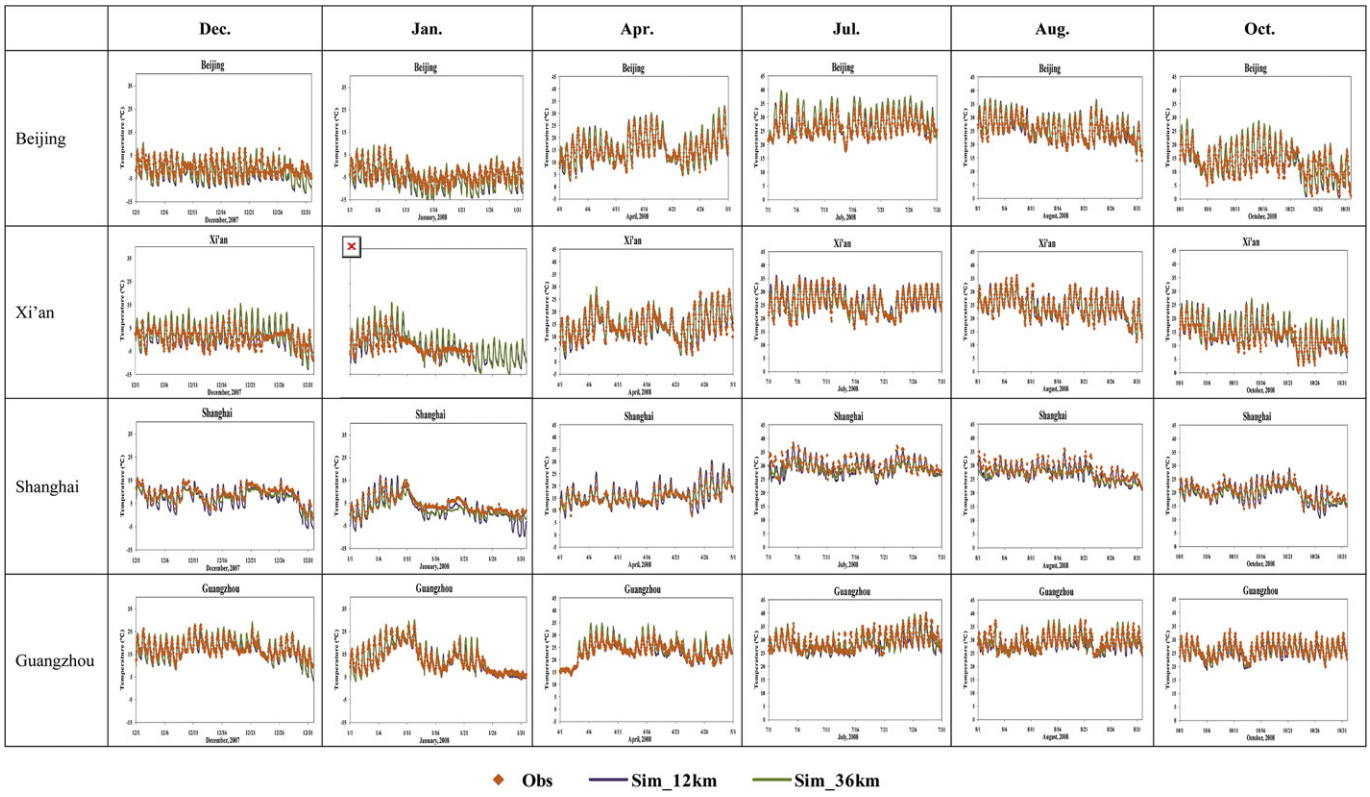


**Fig. 4.** Observed and simulated hourly temperature at 2-m in Beijing, Xi'an, Shanghai, and Guangzhou.

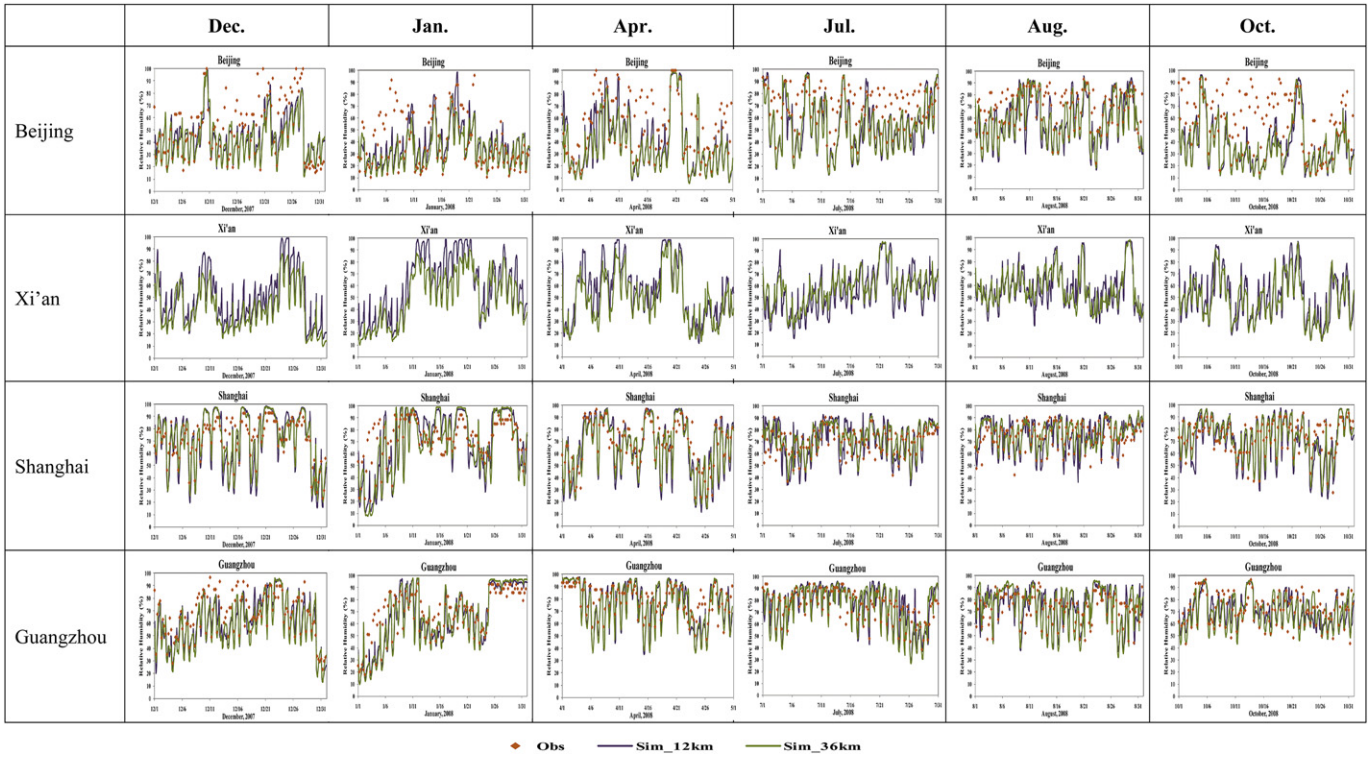


**Fig. 5.** Observed and simulated hourly relative humidity at 2-m in Beijing, Xi'an, Shanghai, and Guangzhou.

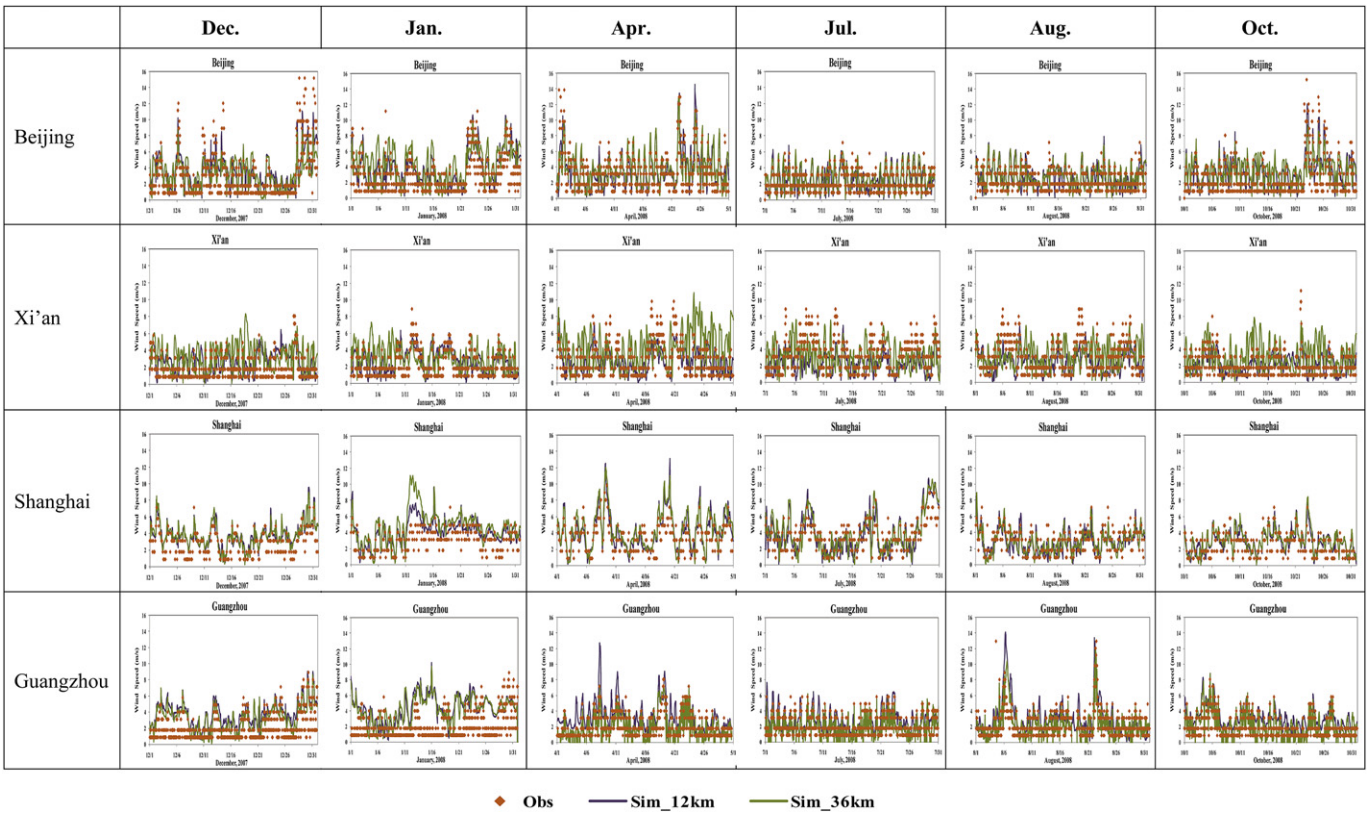


**Fig. 6.** Observed and simulated hourly wind speed at 10-m in Beijing, Xi'an, Shanghai, and Guangzhou.

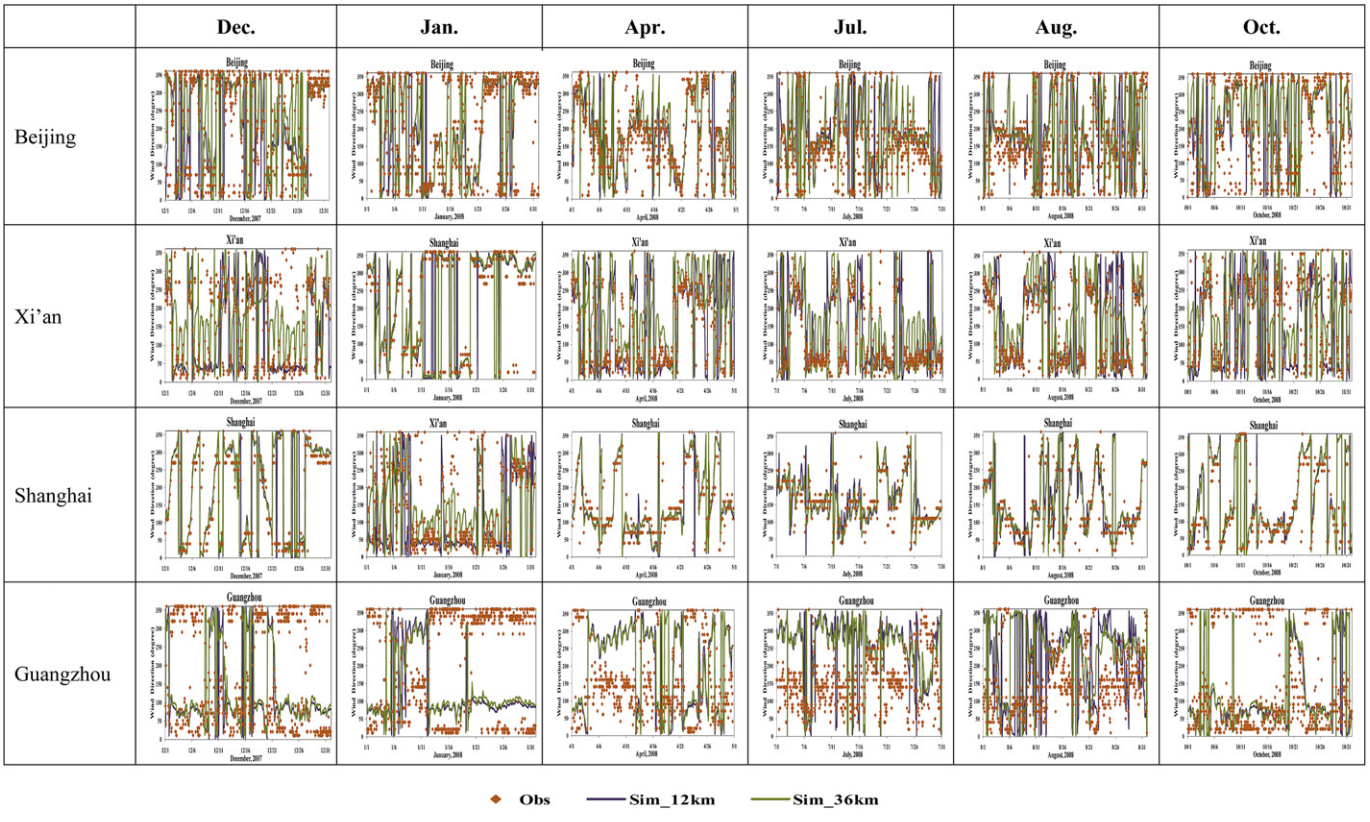


**Fig. 7.** Observed and simulated hourly wind direction at 10-m in Beijing, Xi'an, Shanghai, and Guangzhou.

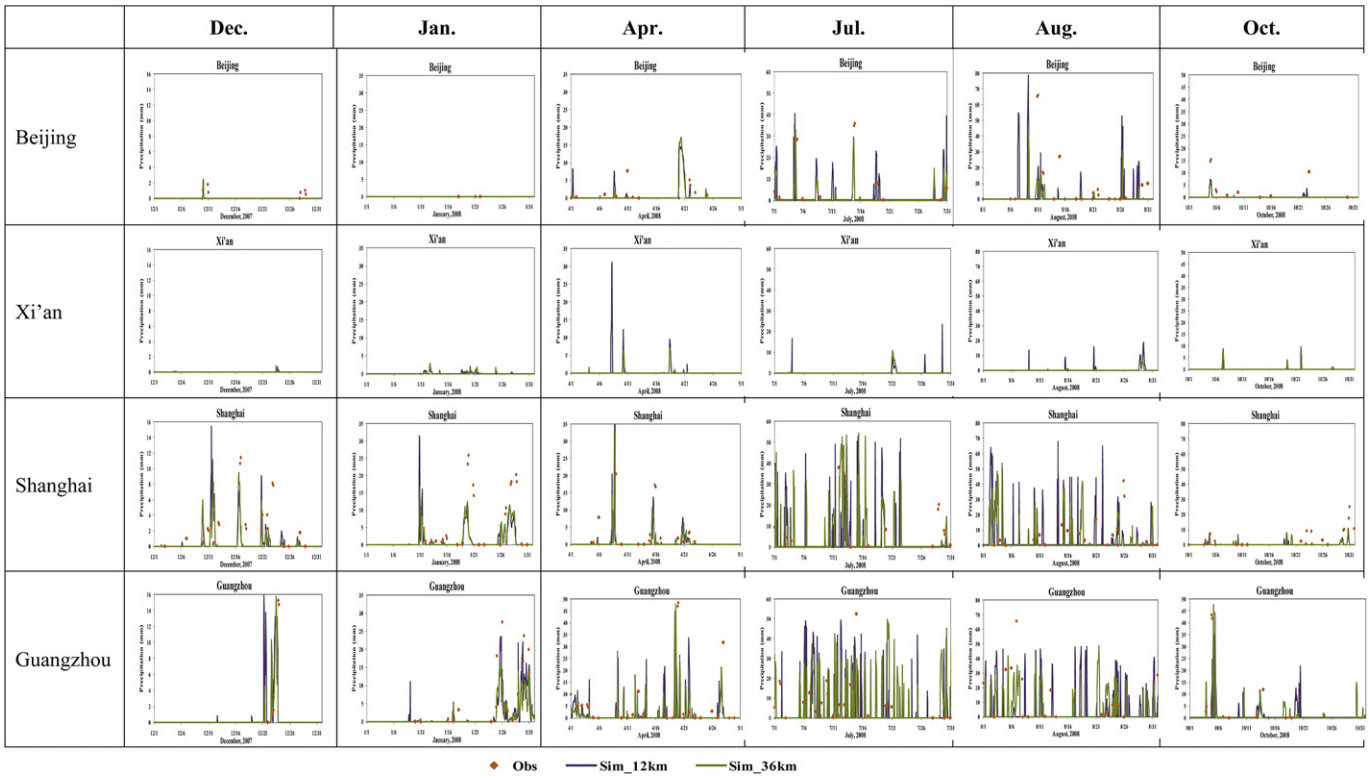


**Fig. 8.** Observed and simulated daily precipitation in Beijing, Xi'an, Shanghai, and Guangzhou.

overestimation in the intensity of the rainfall typically simulated by the Kain-Fritsch cumulus parameterization in summer (Olerud and Sims, 2004). Overall, the MM5 performance in terms of T2, RH2, WSP10, WDR10, and precipitation during the six months is generally consistent with similar applications over other regions (e.g., Wu et al., 2008b; Queen et al., 2008), with good agreement for T2 (for all seasons except for winter), RH2, and WDR10, but relatively poor agreement for T2 in winter and WSP10 and precipitation in the six months.

## 4. Evaluation of winter month simulations at 4-km and model sensitivity to horizontal grid resolutions

### 4.1. Spatial distributions

Fig. 9 shows the spatial distribution of T2, RH2, WSP10, and Precip overlaid with the observations at 4-km for Dec. 2007 and Jan. 2008. Table 4 compares performance statistics over the 4-km domain from simulations at 36-, 12- and 4-km simulations. T2 is underpredicted with MBs of −0.8 °C, particularly in the northwest of Shandong Province in Dec. and over the central domain in Jan. RH2 is underpredicted over the entire domain in both months with MBs ranging from −21.2% to −14.3%. WSP10 is significantly overpredicted over the entire domain in both months with MBs ranging from 1.6 to 1.8 m $s^{-1}$. Precip is underpredicted over most of domain with MBs of −1.3 to −0.7 mm $day^{-1}$. Compared with results at 36- and 12-km, the model predictions are not improved at 4-km, due likely to the low resolution of the land use data used and the difficulty in simulating meteorological processes over a complex terrain consisting of mountains (e.g., Mountain Tai and Mountains in the south of Shandong Province) in the South and oceanic areas in the east of Shandong Province. These results indicate that meteorology modeling at a fine grid resolution do not always show a better performance due to limitations in model treatments and/or inaccuracies in model inputs, consistent with other studies (e.g., Queen et al., 2008; Wu et al., 2008b). Xing et al. (2011) conducted MM5 simulations for August 2008 over a different 4-km domain that covers the Beijing area using boundary and initial conditions derived from the MM5 simulation at 12-km in this effort. They found that the model performance at 4-km for summer months is consistent with that of MM5 for summer months in other applications and it is better than that in winter months. For example, the NMBs for MM5 at 4-km for August 2008 are 4% for T2, −6% for RH2, 19% for WSP10, 6% for WDR10, and 15% for precipitation.

### 4.2. Temporal variations

Temporal analyses are conducted at three selected sites where observational data are available: Jinan, Qingdao, and Taishan in the 4-km domain. Jinan is the capital of Shandong Province and represents an urban site, Qingdao is a coastal site, and Taishan is a mountain site with an elevation of 1500 m above the sea level. As shown in Fig. 10, maximum T2 is overpredicted and minimum T2 is underpredicted in both months in Jinan. At Taishan, MM5 can capture the variation of observed temperatures but significantly overpredict their magnitudes due to the complexity of terrain (Ma et al., 2008). In Qingdao, MM5 reproduces well maximum T2 but underpredicts minimum T2 in both. Among the three simulations, the 4-km simulation gives the best agreement for T2 at Taishan site. Maximum RH2 predictions in Jinan and Qingdao agree well with observations but minimum RH2 is underpredicted in both months. Better agreement in terms of magnitudes and variation trends in RH2 is found at Taishan. Among the three simulations, the 4-km simulation gives the best agreement for RH2 at all sites. MM5 reproduces observed maximum WSP10 in Jinan and Qingdao but underpredicts maximum WSP10 at Taishan and overpredicts minimum WSP10 at Jinan and Qingdao. Large deviation in WDR10 occurs at all sites, particularly in Jan. The 4-km simulation shows

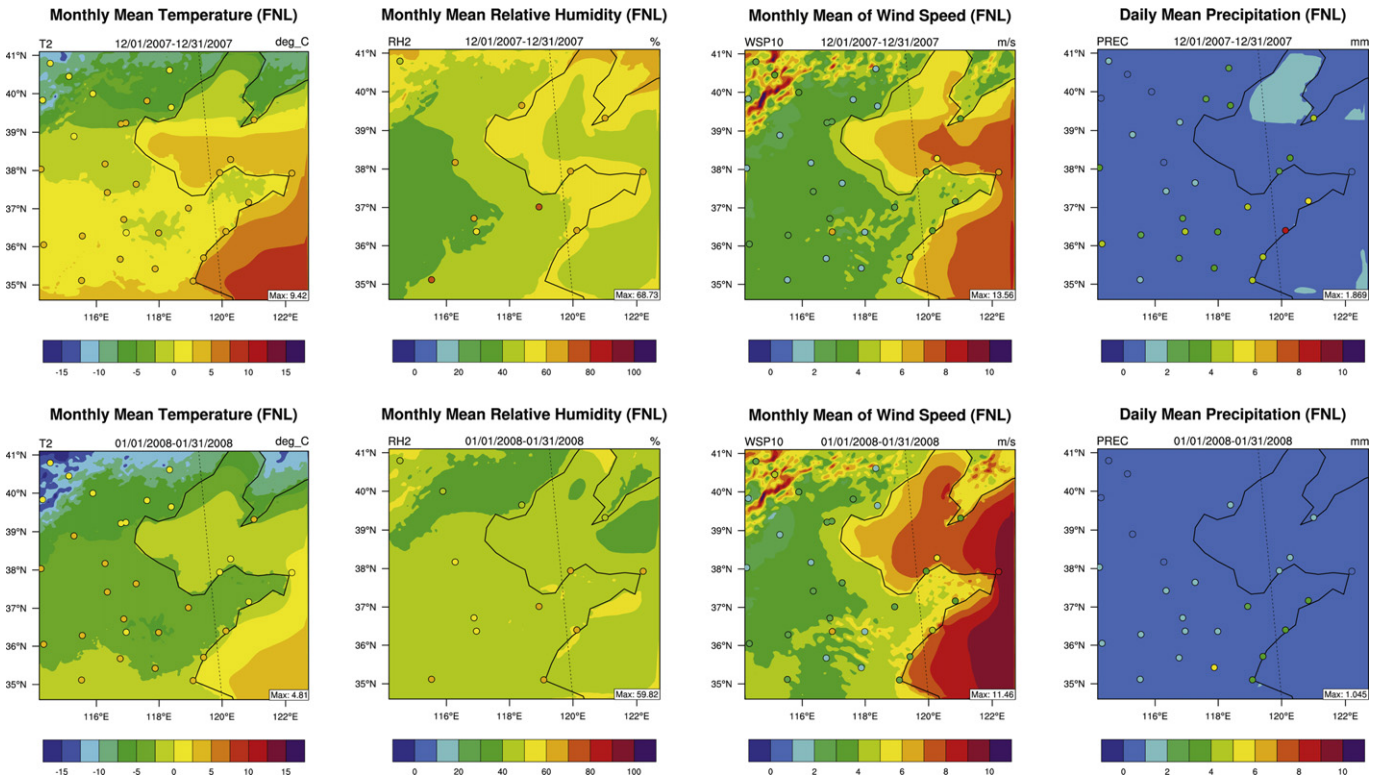


**Fig. 9.** Spatial distribution of T2, RH2, WSP10 and Precip at 4-km overlaid with observation.

**Table 4**
Performance statistics of MM5 simulations at 36-, 12- and 4-km over the 4-km domain.

| | Month | Grid size (km) | MeanObs | MeanMod | $R^a$ | MB[a] | RMSE[a] | NMB(%)[a] | NME(%)[a] |
|---|---|---|---|---|---|---|---|---|---|
| T2 | Dec | 4 | 3.9 | 3.1 | 0.7 | −0.8 | 3.3 | −20 | 70 |
| | | 12 | 3.9 | 3.5 | 0.7 | −0.4 | 3.1 | −10 | 60 |
| | | 36 | 3.9 | 3.5 | 0.7 | −0.4 | 2.7 | −10 | 50 |
| | Jan | 4 | 3.3 | 2.5 | 0.7 | −0.8 | 2.8 | −20 | 60 |
| | | 12 | 3.3 | 3.0 | 0.7 | −0.3 | 2.8 | −10 | 60 |
| | | 36 | 3.3 | 2.6 | 0.7 | −0.7 | 2.5 | −20 | 60 |
| RH2 | Dec | 4 | 64.7 | 43.6 | 0.5 | −21.2 | 30.0 | −30 | 40 |
| | | 12 | 64.7 | 44.7 | 0.5 | −20.1 | 29.6 | −30 | 40 |
| | | 36 | 64.7 | 46.4 | 0.5 | −18.3 | 28.9 | −30 | 40 |
| | Jan | 4 | 58.2 | 43.9 | 0.6 | −14.3 | 23.0 | −20 | 30 |
| | | 12 | 58.2 | 42.9 | 0.6 | −15.4 | 24.6 | −30 | 30 |
| | | 36 | 58.2 | 48.6 | 0.6 | −9.6 | 20.3 | −20 | 30 |
| WSP10 | Dec | 4 | 2.8 | 4.4 | 0.6 | 1.6 | 2.7 | 50 | 80 |
| | | 12 | 2.8 | 4.7 | 0.6 | 1.8 | 3.0 | 60 | 80 |
| | | 36 | 2.8 | 4.2 | 0.6 | 1.3 | 2.7 | 50 | 70 |
| | Jan | 4 | 3.0 | 4.8 | 0.6 | 1.8 | 2.8 | 60 | 80 |
| | | 12 | 3.0 | 4.4 | 0.6 | 1.4 | 2.6 | 50 | 70 |
| | | 36 | 3.0 | 5.0 | 0.6 | 2.0 | 3.1 | 70 | 80 |
| WDR10 | Dec | 4 | 231.1 | 153.5 | 0.0 | −77.6 | 193.6 | −30 | 60 |
| | | 12 | 231.1 | 150.2 | 0.0 | −80.9 | 193.4 | −40 | 60 |
| | | 36 | 231.1 | 218.7 | 0.3 | −12.5 | 166.6 | −10 | 40 |
| | Jan | 4 | 210.5 | 183.3 | 0.3 | −27.2 | 171.4 | −10 | 50 |
| | | 12 | 210.5 | 189.7 | 0.3 | −20.9 | 172.6 | −10 | 50 |
| | | 36 | 210.5 | 186.5 | 0.3 | −24.1 | 172.7 | −10 | 50 |
| Precip | Dec | 4 | 2.8 | 1.5 | 0.1 | −1.3 | 5.0 | −50 | 110 |
| | | 12 | 2.8 | 2.0 | 0.2 | −0.8 | 5.0 | −30 | 110 |
| | | 36 | 2.8 | 1.7 | 0.2 | −1.1 | 4.6 | −40 | 110 |
| | Jan | 4 | 2.3 | 1.6 | 0.3 | −0.7 | 4.2 | −30 | 100 |
| | | 12 | 2.3 | 1.6 | 0.2 | −0.8 | 3.9 | −30 | 100 |
| | | 36 | 2.3 | 2.0 | 0.3 | −0.3 | 3.9 | −10 | 100 |

Precip – Precipitation, RH2 – 2 m Relative Humidity, T2 – 2 m Temperature, WDR10 – 10 m Wind Direction, WSP10 – 10 m Wind Speed.
[a] $R$ – Correlation Coefficient, MB – Mean Bias, RMSE – Root Mean Square Error, NMB – Normalized mean bias, NME – Normalized mean error.

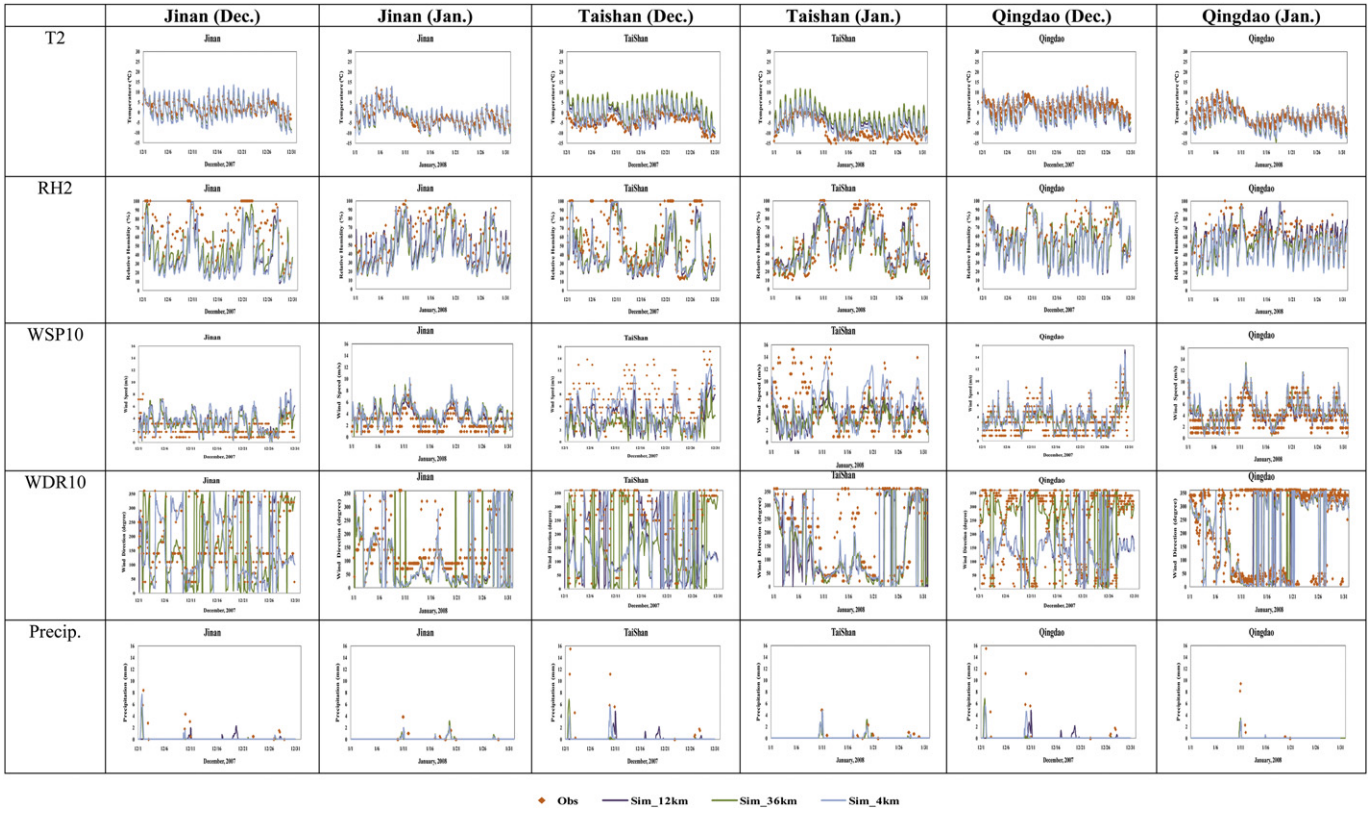


**Fig. 10.** Time series plots of T2, RH2, WSP10, WDR10 and Precip. in Jinan, Taishan and Qingdao for Dec., 2007 and Jan., 2008.

the closest agreement with observed WSP10 and WDR10 among the three simulations. Precipitation amounts are well predicted at Taishan in January but are underpredicted in Jinan and Qingdao in both months and in Taishan in December. Simulations at different grid resolutions give different amounts of Precip at different times (e.g., at all three sites in Dec.), indicating a high sensitivity.

## 5. Summary

MM5 is applied to China with the PX-LSM model and three different nudging over triple-nested domains. Performance statistics show that simulated T2, RH2, WSP10, and WDR10 agree with observations better in summer than in winter, while the precipitation shows worse performance in summer. The model performance in April and October is similar. Simulated T2, RH2 and WSP10 agree more closely with observations in the eastern China. For the 36-km simulation, T2 is underpredicted in the western and northern China, especially in winter, due likely to the model difficulties in simulating complex terrain and snow cover. RH2 is underpredicted in all months except for Jan. WSP10 is overpredicted, particularly in the western and northern China. Precipitation is underpredicted in the most of China. Temporal analyses in the four major cities show the MM5 simulations at 36-km during the six months capture well the observed T2 during spring, summer, and fall, but perform relatively poor in reproducing wind speed and precipitation. In winter, MM5 cannot capture well the maximum or minimum T2 and RH2. Further temporal analyses at specific sites show that the meteorological predictions such as T2 and WSP10 agree more closely with observations at urban sites than those at the coastal and mountain sites where the model performance deteriorates because of the complex terrains, higher elevations, and influences of local meteorological processes such as urban heat island effect and land/sea breezes. Model evaluation shows that the 12-km simulation performs better while the 4-km simulation shows the worst performance due to the inaccuracies in the land use and terrain information at 4-km as well as limitations of model treatments (e.g., PBL and land-surface schemes) at a fine grid scale. These results have important implications on air quality and regional haze predictions in China.

## Acknowledgments

This project was supported by China Scholarship Council at Shandong University, China and the U.S. NSF Career Award No. Atm-0348819 at NCSU. Thanks are due to Doug Schuster and Gregg Walters, the U.S. NCAR, for providing the method and revised scripts (download from the website) to process the observational nudging data for MM5 simulations. Thanks are also due to Jonathan Pleim and Robert Gilliam, the U.S. EPA, for providing MM5 with deep soil nudging and useful suggestions on model set up.

## References

Andreae, M.O., Schmid, O., Yang, H., 2008. Optical properties and chemical composition of the atmospheric aerosol in urban Guangzhou, China. Atmospheric Environment 42, 6335–6350.

Athanassiadis, G.A., Rao, S.T., Ku, J.Y., Clark, R.D., 2002. Boundary layer evaluation and its influence on ground-level ozone concentrations. Environmental Fluid Mechanics 2, 339–357.

Betts, A.K., Chen, F., Mitchell, K.E., Janjic, Z.I., 1997. Assessment of the land surface and boundary layer models in two operational versions of the NCEP Eta model using FIFE data. Monthly Weather Review 125, 2896–2916.

Cao, J.J., Lee, S.C., Ho, K.F., Zou, S.C., Fung, K., Li, Y., Watson, J.G., Chow, J.C., 2004. Spatial and seasonal variations of atmospheric organic carbon and elemental carbon in Pearl River Delta Region, China. Atmospheric Environment 38, 4447–4456.

Franke, K., Ansmann, A., Muller, D., 2003. Optical properties of Indo-Asian haze layer over the tropical Indian Ocean. Journal of Geophysical Research 108, 4059.

Gao, H., 2009. China's snow disaster in 2008, who is the principal player? International Journal of Climatology. doi:10.1002/joc.1859.

Garland, R.M., Yang, H., Schmid, O., Rose, D., Nowak, A., Achtert, P., Wiedensohler, A., Takegawa, N., Kita, K., Miyazaki, Y., Kondo, Y., Hu, M., Shao, M., Zeng, L.M., Zhang, Y.H., Andreae, M.O., Pöschl, U., 2008. Aerosol optical properties in a rural environment near the mega-city Guangzhou, China: implications for regional air pollution, radiative forcing and remote sensing. Atmospheric Chemistry and Physics 8, 5161–5186.

Ge, G., 2008. The climatic characteristics and change of haze days over China during 1961–2005. Acta Geographica Sinica 2008-07, DOI: CNKI:SUN:DLXB.0.2008-07-013.

Hagler, G.S.W., Bergin, M.H., Salmon, L.G., Yu, J.Z., Wan, E.C.H., 2006. Source areas and chemical composition of fine particulate matter in the Pearl River Delta region of China. Atmospheric Environment 40, 3802–3815.

Jung, J., Lee, H., Kim, Y.J., Liu, X.-G., Zhang, Y.-H., Gu, J.-W., Fan, S.-J., 2009. Aerosol chemistry and the effect of aerosol water content on visibility impairment and radiative forcing in Guangzhou during the 2006 Pearl River Delta campaign. Journal of Environmental Management 90, 3231–3244.

Kaiser, D.P., Qian, Y., 2002. Decreasing trends in sunshine duration over China for 1954–1998: indication of increased haze pollution? Geophysical Research Letters 29, 2042.

Koe, LC.C., Arellano, A.F., McGregor Jr., J.L., 2001. Investigating the haze transport from 1997 biomass burning in Southeast Asia its impact upon Singapore. Atmospheric Environment 35, 2723–2734.

Ku, J.Y., Mao, H., Zhang, K., Civerolo, K., Rao, S.T., Philbrick, C.R., Doddridge, B., Clark, R., 2001. Numerical investigation of the effects of boundary-layer evolution on the predictions of ozone and the efficacy of emission control options in the northeastern United States. Environmental Fluid Mechanics 1, 209–233.

Liu, X.-H., Zhang, Y., Cheng, S.-H., Xing, J., Zhang, Q., Streets, D.G., Jang, C.J., Wang, W.-X., Hao, J.-M., 2010a. Understanding of regional air pollution over China using CMAQ, part I performance evaluation and seasonal variation. Atmospheric Environment 44 (20), 2415–2426.

Liu, X.-H., Zhang, Y., Xing, J., Zhang, Q., Wang, K., Streets, D.G., Jang, C.J., Wang, W.-X., Hao, J.-M., 2010b. Understanding of regional air pollution over china using CMAQ, part II. Process analysis and ozone sensitivity to precursor emissions. Atmospheric Environment 44 (20), 3719–3727.

Ma, L.-J., Zhang, T.-J., Li, Q.-X., Frauenfeld, O.W., Qin, D., 2008. Evaluation of ERA-40, NCEP-1, and NCEP-2 reanalysis air temperatures with ground-based measurements in China. Journal of Geophysical Research 113 (D15115).

Miao, J.-F., Chen, D., Borne, K., 2007. Evaluation and comparison of Noah and Pleim-Xiu land surface models in MM5 using GOTE2001 data: spatial and temporal variations in near-surface air temperature. Journal of Applied Meteorology and Climatology 46 (10), 1587–1605.

Miao, J.-F., Chen, D., Wyser, K., Borne, K., Lindgren, J., Strandevall, M.K.S., Thorsson, S., Achberger, C., Almkvist, E., 2008. Evaluation of MM5 mesoscale model at local scale for air quality applications over the Swedish west coast: influence of PBL and LSM parameterizations. Meteorology and Atmospheric Physics 99, 77–103.

Mitra, A.P., Sharma, C., 2002. Indian aerosols: present status. Chemosphere 49, 1175–1190.

Misenis, C., Zhang, Y., 2010. An examination of WRF/Chem: physical parameterizations, nesting options, and grid resolutions. Atmospheric Research 97, 315–334.

Olerud, D., Sims, A., 2004. MM5 2002 Modeling in Support of VISTAS (Visibility Improvement – State and Tribal Association of the Southeast). http://www.baronams.com/projects/VISTAS/reports/VISTAS_TASK3f_final.pdf.

Pino, D., Vil a-Guerau de Arellano, J., Comeron, A., Rocadenbosch, F., 2004. The boundary layer growth in an urban area. Science of Total Environment 334–335, 207–213.

Pleim, J.E., Xiu, A., 1995. Development and testing of a surface flux and planetary boundary layer model for application in mesoscale models. Journal of Applied Meteorology 34, 16–32.

Pleim, J.E., Xiu, A., Finkelstein, P.L., Otte, T.L., 2001. A coupled land-surface and dry deposition model and comparison to field measurements of surface heat, moisture, and ozone fluxes. Water, Air, and Soil Polution: Focus 1, 243–252.

Pope, C.A., Burnett, R.T., Thurston, G.D., 2004. Cardiovascular mortality and long-term exposure to particulate air pollution: epidemiological evidence of general pathophysiological pathways of disease. Circulation 109 (1), 71–77.

Queen, A., Zhang, Y., Gilliam, R., Pleim, J., 2008. Examining the sensitivity of MM5–AMAQ predictions to explicit, microphysics schemes, part I—database description, evaluation protocol and precipitation predictions. Atmospheric Environment 42 (16), 3842–3855.

Radojevic, M., 2003. Chemistry of forest fires and regional haze with emphasis on Southeast Asia. Pure and Applied Geophysics. 160, 157–187.

Ramanathan, V., Crutzen, P.J., Lelieveld, J., Mitra, A.P., Althausen, D., Anderson, J., Andreae, M.O., Cantrell, W., Cass, G.R., Chung, C.E., Clarke, A.D., Coakley, J.A., Collins, W.D., Conant, W.C., Dulac, F., Heintzenberg, J., Heymsfield, A.J., Holben, B., Howell, S., Hudson, J., Jayaraman, A., Kiehl, J.T., Krishnamurti, T.N., Lubin, D., McFarquhar, G., Novakov, T., Ogren, J.A., Podgorny, I.A., Prather, K., Priestley, K., Prospero, J.M., Quinn, P.K., Rajeev, K., Rasch, P., Rupert, S., Sadourny, R., Satheesh, S.K., Shaw, G.E., Sheridan, P., Valero, F.P.J., 2001. Indian Ocean experiment: an integrated analysis of the climate forcing and effects of the great Indo-Asia haze. Journal of Geophysical Research 106, 28,371–28,398. doi:10.1029/2001JD900133.

Rose, D., Nowak, A., Achtert, P., Wiedensohler, A., Hu, M., Shao, M., Zhang, Y., Andreae, M.O., Pöschl, U., 2010. Cloud condensation nuclei in polluted air and biomass burning smoke near the mega-city Guangzhou, China Part 1: size-resolved measurements and implications for the modeling of aerosol particle hygroscopicity and CCN activity. Atmospheric Chemistry and Physics 10, 3365–3383. doi:10.5194/acp-10-3365-2010.

Tan, J.H., Duan, J.C., Chen, D.H., Wang, X.-H., Guo, S.-J., Bi, X.-H., Sheng, G.-Y., He, K.-B., Fu, J.-M., 2009. Chemical characteristics of haze during summer and winter in Guangzhou. Atmospheric Research 94, 238–245.

United Nations Environmental Program (UNEP) and the Center for Clouds, Chemistry and Climate ($C^4$), 2002. The Asian Brown Cloud: Climate and Other Environmental Impacts UNEP, Nairobi, Report Commissioned by the United Nations Environment Programme (UNEP) and Prepared by the Center for Clouds, Chemistry and Climate (C4), Funded by the UNEP, National Science Foundation, USA, the G. Unger Vetlesen, Foundation, and the Alderson Chair Funds to the Scripps Institution of Oceanography. University of California, San Diego, ISBN 92-807-2240-9. United Nations Environment Programme, Klong Luang, Pathumthani 12120, Thailand.

Wang, K., Zhang, Y., Jang, C.J., Phillips, S., Wang, B.-Y., 2009. Modeling study of Intercontinental air pollution transport over the Trans-Pacific region in 2001 using the Community Multiscale Air Quality (CMAQ) modeling system. Journal of Geophysical Research 114 (D04307). doi:10.1029/2008JD010807.

Wang, T., Cheung, T.F., Li, Y.S., 2002. Emission characteristics of CO, NOx, $SO_2$ and indications of biomass burning observed at a rural site in eastern China. Journal of Geophysical Research 107, 4157.

Wang, T., Poon, C.N., Kwok, Y.H., Li, Y.S., 2003. Characterizing the temporal variability and emission patterns of pollution plumes in the Pearl River Delta of China. Atmospheric Environment 37, 3539–3550.

Wang, H.-X., Zhou, L.-J., Tang, X.-Y., 2006. Ozone concentrations in rural regions of the Yangtze Delta in China. Journal of Atmospheric Chemistry 54, 255–265.

Wu, D., 2005. A discussion on the difference between haze and fog and the warning of ash haze weather. Meteorological Monograph 31 (4), 3–7 (In Chinese).

Wu, D., 2006. More discussions on the differences between haze and fog in city. Meteorological Monograph 32 (4), 9–15 (In Chinese).

Wu, D., Bi, X.-Y., Deng, X.-J., Li, F., Tan, H.-B., Liao, G.-L., Huang, J., 2008a. Effect of atmospheric haze on the deterioration of visibility over the Pearl River Delta. Acta Meteorologica Sinica 21, 215–222.

Wu, S.-Y., Krishnan, S., Zhang, Y., Aneja, V., 2008b. Modeling atmospheric transport and fate of ammonia in North Carolina, Part I. Evaluation of meteorological and chemical predictions. Atmospheric Environment 42, 3419–3436.

Xiao, R., Takegawa, N., Kondo, Y., Miyazaki, Y., Miyakawa, T., Hu, M., Shao, M., Zeng, L.M., Hofzumahaus, A., Holland, F., Lu, K., Sugimoto, N., Zhao, Y., Zhang, Y.H., 2009. Formation of submicron sulfate and organic aerosols in the outflow from the urban region of the Pearl River Delta in China. Atmospheric Environment 43, 3754–3763.

Xing, J., Zhang, Y., Wang, S.-X., Liu, X.-H., Cheng, S.-H., Zhang, Q., Chen, Y.-S., Streets, D.G., Jang, C., Hao, J.-M., Wang, W.-X., 2011. Modeling study on the air quality impacts from emission reductions and atypical meteorological conditions during the 2008 Beijing Olympics. Atmospheric Environment 45, 1786–1798.

Xiu, A., Pleim, J.E., 2001. Development of a land surface model part I: application in a mesoscale meteorology model. Journal of Applied Meteorology 40, 192–209.

Ye, B.-M., Ji, X.-L., Yang, H.-Z., Yao, X.-H., Chan, C.K., Cadle, S.H., Chan, T., Mulawa, P.A., 2003. Concentration and chemical composition of $PM_{2.5}$ in Shanghai for a 1-year period. Atmospheric Environment 37, 499–510.

Yu, S., Saxena, V.K., Zhao, Z., 2001. A comparison of signals of regional aerosol-induced forcing in eastern China and the southeastern United States. Geophysical Research Letters 28, 713–716.

Yu, H., Wu, C., Wu, D., Yu, J.Z., 2010. Size distributions of elemental carbon and its contribution to light extinction in urban and rural locations in the pearl river delta region, China. Atmospheric Chemistry and Physics 10, 5107–5119.

Yue, D.L., Hu, M., Wu, Z.J., Guo, S., Wen, M.T., Nowak, A., Wehner, B., Wiedensohler, A., Takegawa, N., Kondo, Y., Wang, X.S., Li, Y.P., Zeng, L.M., Zhang, Y.H., 2010. Variation of particle number size distributions and chemical compositions at the urban and downwind regional sites in the Pearl River Delta during summertime pollution episodes. Atmospheric Chemistry and Physics 10, 9431–9439.

Zhang, K., Mao, H., Civerolo, K., Berman, S., Ku, J.Y., Rao, S.T., Doddridge, B., Philbrick, C.R., Clark, R., 2001. Numerical investigation of boundary-layer evolution and nocturnal low-level jets: local versus non-local PBL schemes. Environmental Fluid Mechanics 1, 171–208.

Zhang, X.Y., Cao, J.J., Li, L.M., Arimoto, R., Cheng, Y., Huebert, B., Wang, D., 2002. Characterization of atmospheric aerosol over XiAn in the south margin of the Loess Plateau, China. Atmospheric Environment 36, 4189–4199.

Zhang, Y., Liu, P., Pun, B., Seigneur, C., 2006. A comprehensive performance evaluation of MM5–CMAQ for summer 1999 southern oxidants study episode, Part-I. Evaluation protocols, databases and meteorological predictions. Atmospheric Environment 40, 4825–4838.